DOI: 10.61782/fa.2025.0333

FORUM ACUSTICUM
EURONOISE 2025

EFFICIENT SIMULATION OF TIME-DOMAIN ACOUSTIC WAVE PROPAGATION IN UNBOUNDED AND PENETRABLE MEDIA

Víctor Domínguez [1*] **Mahadevan Ganesh**[2] **Frédérique Le Louër**[3]

[1] Department of Estadística, Informática y Matemática,
Universidad Pública de Navarra, Spain
[2] Department of Applied Mathematics & Statistics, Colorado School of Mines, USA.
[3] Laboratoire de Mathématiques Appliquées de Compiègne,
Alliance Sorbonne Université, Université de Technologie de Compiègne, France

ABSTRACT

Space- and time-dependent acoustic wave propagation naturally occurs in unbounded regions with discontinuous velocity fields. These unbounded regions typically consist of free space (which has a constant propagation speed) and a penetrable bounded medium, where the propagation speed differs from that of the surrounding unbounded environment. Standard approaches for simulating the time-domain model of penetrable media include: (i) truncating the unbounded region with an artificial boundary condition; or (ii) ignoring the penetrable properties of the bounded medium. The first approach usually employs the finite element method (FEM) in space, combined with time-stepping discretization. In contrast, the second approach leverages the analytical representation of the Green's function of the time-domain model in free space. This allows the boundary element method (BEM) in space, along with convolution quadrature (CQ), to efficiently simulate the exterior model.

Building on our recent work involving a high-order BEM-CQ model for the time-domain free-space model and an overlapped frequency-domain FEM-BEM framework, in this article we propose and demonstrate an efficient simulation framework for time-domain acoustic wave propagation in unbounded and penetrable media.

*__Corresponding author__: *victor.dominguez@unavarra.es.*

Keywords: *Wave propagation, Convolution-Quadrature, Boundary and Finite Element Methods*

1. INTRODUCTION

Simulating the time-dependent scattered and absorbed waves in unbounded free space and within a bounded penetrable medium is fundamental to numerous applications, as indicated in the literature [1–4]. This simulation addresses the waves resulting from an incident wave that strikes the boundary of the penetrable domain.

To efficiently simulate the scattered and absorbed fields, it is crucial to accurately retain two key physical properties of the time-domain model: the existence of the unbounded region and the penetrable medium. Although there is substantial literature on simulating the penetrable time-domain model using the FEM [3], this approach often neglects the propagation of scattered waves throughout the entire free space. Alternatively, the BEM and CQ can be employed to accommodate unbounded domains; however, these methods typically overlook the penetrable nature of the bounded medium [2].

For discretization in the time variable, CQ methods were introduced by C. Lubich in his seminal paper [5], which focused on convolution equations related to parabolic problems. Since then, CQ methods have proven to be a powerful tool for simulating transient wave problems (see [2] for a comprehensive introduction). Essentially, CQ methods utilize ordinary differential equation (ODE) solvers directly in the Laplace domain to achieve stable time discretization of the problem.

In comparison to the time-stepping discretization

used with FEM sparse matrices for the truncated domain model, the CQ-BEM results in complex dense matrices and necessitates the discretization of a large number of associated frequency-domain (FD) Helmholtz elliptic partial differential equations (PDEs) [2], which proves to be prohibitively expensive when utilizing low-order BEM. In a recent study [6], the authors developed a practical CQ-BEM model for the impenetrable unbounded media time-domain model by employing their spectrally accurate discretization of the FD-PDE in conjunction with high-order CQ.

In this article, we extend this approach to a piecewise-constant penetrable media time-dependent model, demonstrating high-order accuracy and efficiency. Generally, the penetrable media encompasses continuously spatially varying heterogeneity. Following our FD Helmholtz overlapped FEM-BEM framework [7, 8], we plan to develop and analyze a TD-FEM-BEM-CQ framework in future work. In this article, we also provide preliminary numerical results from this framework and compare these results with the spectral CQ-BEM for the restricted piecewise-constant media model. For numerical experiments, we adopt a parallel implementation of CQ that avoids the explicit computation of the weights characterizing the method.

2. ACOUSTIC WAVE PROPAGATION PROBLEM

In this article, we consider the solution to the following transient wave transmission problem in $\mathbb{R}^d$ where $d = 2$ or 3. Let $c : \mathbb{R}^d \to \mathbb{R}^+$ denote a discontinuous function representing a known velocity field. Let $\Omega \subset \mathbb{R}^d$ be a bounded, wave-penetrable domain, such that its complement $\Omega^c = \mathbb{R}^d \setminus \overline{\Omega}$ represents the free space where the wave speed is constant, denoted as c_0. Specifically, we have $c(\mathbf{x}) = c_0$ for all $\mathbf{x} \in \Omega^c$, and c is at least discontinuous along the boundary $\partial\Omega$ of the penetrable region Ω. In this article, we allow for $c(\mathbf{x}) \neq c_0$ for all $\mathbf{x} \in \overline{\Omega}$.

The propagation of waves in $\mathbb{R}^d$ is induced by a time-dependent incident wave $u^{\text{inc}}(t, \mathbf{x})$ originating from the free space and not yet impacting Ω at $t = 0$. In particular the input incident field satisfies the homogeneous wave equation in homogeneous media:

$$\ddot{u}^{\text{inc}} = c_0^2 \Delta u^{\text{inc}}, \quad u^{\text{inc}}(0, \cdot) = \dot{u}^{\text{inc}}(0, \cdot) = 0 \ \text{ in } \mathbb{R}^d.$$

The resulting time-domain wave propagation model for the total field $u^{\text{tot}} = u^{\text{inc}} + u$ satisfies the classical wave equation, with the unknown field $u(t, \mathbf{x})$ defined for all $\mathbf{x} \in \mathbb{R}^d$. In particular, u satisfies the inhomogeneous wave equation for $t \in (0, T]$:

$$\frac{1}{c^2}\ddot{u}(t) = \Delta u(t) + f(t), \quad u(0, \cdot) = 0, \quad \dot{u}(0, \cdot) = 0 \ \text{ in } \mathbb{R}^d,$$

where

$$f = -c^{-2}\ddot{u}^{\text{inc}} + \Delta u^{\text{inc}} = \left(1 - \frac{c_0^2}{c^2}\right) \Delta u^{\text{inc}}.$$

We note that $f(t, \mathbf{x}) = 0$ for all $\mathbf{x} \in \Omega^c$ and $t \in [0, T]$, a property that will be essential in formulating our TD-FEM-BEM-CQ method for a general heterogeneous velocity field c. For the specific case of a piecewise-constant velocity field, the above PDE transmission wave propagation model can be reformulated as a coupled system of boundary integral equations (BIE).

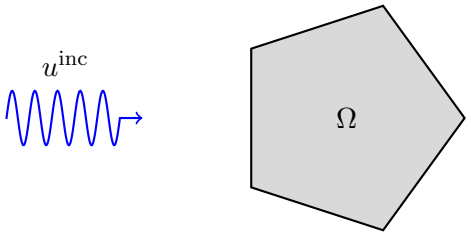

Figure 1. Transient acoustic wave problem

3. COUPLED BIE REFORMULATION

In this section, we assume that the sound speed c takes different positive constant values inside and outside the domain Ω, defined as follows:

$$c(\mathbf{x}) = \begin{cases} c_0 & \text{if } \mathbf{x} \in \Omega^c, \\ c_1 & \text{if } \mathbf{x} \in \Omega. \end{cases} \tag{1}$$

In this case, the total field u^{tot} satisfies two constant coefficient homogeneous wave equations, one in Ω and another in Ω^c. Although the coupled BIE reformulation in this section can be extended to accommodate multiple piecewise-constant speeds of propagation within Ω, it is not practical, for computational purposes, to simulate a larger version of the coupled BIE system presented in this section.

The BIE reformulation requires solving only for unknowns in the boundary region $\partial\Omega$. However, for a general heterogeneous medium Ω, it is efficient to develop an

overlapped decomposition framework that facilitates application of both the FEM and BEM discretization, in conjunction with the Laplace transform (LT)-based CQ approach. In this article, we also demonstrate such an overlapped framework, and compare with the BIE approach for the limited special case (1).

For any constant real value $k > 0$, let

$$G(k,t,\mathbf{z}) = \begin{cases} \dfrac{1}{4\pi\|\mathbf{z}\|}\delta\left(t - \dfrac{\|\mathbf{z}\|}{k}\right), & \text{in 3D,} \\ \dfrac{H(t-k^{-1}\|\mathbf{z}\|)}{2\pi\sqrt{t^2-k^{-2}\|\mathbf{z}\|^2}} & \text{in 2D,} \end{cases} \tag{2}$$

be the fundamental solution of the time-domain wave equation with a constant speed of propagation, say k, in a (bounded or unbounded) region $\widetilde{\Omega}$. Here δ and H denote the Dirac delta and Heaviside functions, respectively. In our case, $\widetilde{\Omega} = \Omega$ or $\widetilde{\Omega} = \Omega^c$. We also denote the outer unit normal vector to $\partial\Omega$ by $\boldsymbol{\nu}$. In this article, we utilize the LT for high-order time discretization that also facilitates transformed parallel-in-time implementation. The coupled BIE reformulation depends on several operators that we will first define below.

For a given density φ and $t > 0,\ \mathbf{x} \in \Omega \cup \Omega^c$, the time-dependent retarded single layer potential operator is defined as

$$\mathcal{S}_k\varphi(t,\mathbf{x}) = \int_0^t \left[\int_{\partial\Omega} G(k,t-\tau,\mathbf{x}-\mathbf{y})\varphi(\tau,\mathbf{y})d\sigma(\mathbf{y})\right] d\tau.$$

The retarded double layer potential operator is defined, for a given density ψ and $t > 0,\ \mathbf{x} \in \Omega \cup \Omega^c$, as

$$\mathcal{D}_k\psi(t,\mathbf{x}) = \int_0^t \left[\int_{\partial\Omega} \frac{\partial G}{\partial\boldsymbol{\nu}(\mathbf{y})}(k,t-\tau,\mathbf{x}-\mathbf{y})\psi(\tau,\mathbf{y})d\sigma(\mathbf{y})\right] d\tau.$$

Notice that, in the 3D case, the surface integral on $\partial\Omega$ must be understood in a suitable sense due to the presence of the Dirac delta in the kernel $G(k,t,\mathbf{z})$.

Taking the exterior and interior Dirichlet and Neumann boundary traces of the potential operators lead to the following trace results connection with boundary integral operators (BIOs), at $\mathbf{x} \in \partial\Omega$:

$$\begin{aligned} \lim_{\varrho\to 0^+}(\mathcal{S}_k\varphi)(t,\mathbf{x}\pm\varrho\boldsymbol{\nu}(\mathbf{x})) &= S_k\varphi(t,\mathbf{x}) \\ \lim_{\varrho\to 0^+}(\mathcal{D}_k\psi)(t,\mathbf{x}\pm\varrho\boldsymbol{\nu}(\mathbf{x})) &= (\pm\tfrac{1}{2}\mathrm{I} + D_k)\psi(t,\mathbf{x}), \\ \lim_{\varrho\to 0^+}\tfrac{\partial}{\partial\boldsymbol{\nu}}(\mathcal{S}_k\varphi)(t,\mathbf{x}\pm\varrho\boldsymbol{\nu}(\mathbf{x})) &= (\mp\tfrac{1}{2}\mathrm{I} + D'_k)\varphi(t,\mathbf{x}), \\ \lim_{\varrho\to 0^+}\tfrac{\partial}{\partial\boldsymbol{\nu}}(\mathcal{D}_k\psi)(t,\mathbf{x}\pm\varrho\boldsymbol{\nu}(\mathbf{x})) &= N_k\psi(t,\mathbf{x}), \end{aligned}$$

where the single-, double-, adjoint-double-, and hypersingular-layer BIOs are, respectively, defined for $t > 0,\ \mathbf{x} \in \partial\Omega$, as

$$\begin{aligned} &S_k\varphi(t,\mathbf{x}) = \\ &\int_0^t \left[\int_{\partial\Omega} G(k,t-\tau,\mathbf{x}-\mathbf{y})\varphi(\tau,\mathbf{y})d\sigma(\mathbf{y})\right] d\tau, \\ &D_k\psi(t,\mathbf{x}) = \\ &\int_0^t \left[\int_{\partial\Omega} \frac{\partial G}{\partial\boldsymbol{\nu}(\mathbf{y})}(k,t-\tau,\mathbf{x}-\mathbf{y})\psi(\tau,\mathbf{y})d\sigma(\mathbf{y})\right] d\tau, \\ &D'_k\varphi(t,\mathbf{x}) = \\ &\int_0^t \left[\int_{\partial\Omega} \frac{\partial G}{\partial\boldsymbol{\nu}(\mathbf{x})}(k,t-\tau,\mathbf{x}-\mathbf{y})\varphi(\tau,\mathbf{y})d\sigma(\mathbf{y})\right] d\tau, \\ &N_k\psi(t,\mathbf{x}) = \\ &\int_0^t \left[\int_{\partial\Omega} \frac{\partial^2 G}{\partial\boldsymbol{\nu}(\mathbf{x})\partial\boldsymbol{\nu}(\mathbf{y})}(k,t-\tau,\mathbf{x}-\mathbf{y})\psi(\tau,\mathbf{y})d\sigma(\mathbf{y})\right] d\tau. \end{aligned}$$

For the special case of the velocity field given by (1), we represent the total field u^{tot}, which is a solution of the wave equation in the exterior and interior regions, using the single- and double-layer retarded potential operators. This representation involves unknowns defined only on the boundary $\partial\Omega$. For any $t \geq 0$, we have:

$$(u^{\text{tot}} - u^{\text{inc}})\big|_{\Omega^c} = \mathcal{D}_{c_0}u^{\text{tot}}\big|_{\partial\Omega} - \mathcal{S}_{c_0}\left(\tfrac{\partial u^{\text{tot}}}{\partial\boldsymbol{\nu}}\right)\big|_{\partial\Omega}, \tag{3a}$$

$$u^{\text{tot}}\big|_{\Omega} = \mathcal{S}_{c_1}\left(\tfrac{\partial u^{\text{tot}}}{\partial\boldsymbol{\nu}}\right)\big|_{\partial\Omega} - \mathcal{D}_{c_1}u^{\text{tot}}\big|_{\partial\Omega}. \tag{3b}$$

We recall that in the interior, $u^{\text{tot}}\big|_{\Omega} = u$, and in the exterior, $u = \left(u^{\text{tot}} - u^{\text{inc}}\right)\big|_{\Omega^c}$. The representation above for the TD model with (1) is inspired by a similar direct method representation for the FD Helmholtz transmission problem with a radiation condition, as investigated in [9, Section 4.2].

By subtracting the exterior traces from (3a) and the interior traces from (3b), we obtain the following system of BIEs for the coupled unknown densities defined on the boundary $\varphi = u^{\text{tot}}\big|_{\partial\Omega}$ and $\psi = \left(\tfrac{\partial u^{\text{tot}}}{\partial\boldsymbol{\nu}}\right)\big|_{\partial\Omega}$:

$$\begin{aligned} u^{\text{inc}}\big|_{\partial\Omega} &= \left(\mathrm{I} + D_{c_1} - D_{c_0}\right)\varphi + \left(S_{c_0} - S_{c_1}\right)\psi, \\ \left(\frac{\partial u^{\text{inc}}}{\partial\boldsymbol{\nu}}\right)\big|_{\partial\Omega} &= \left(N_{c_1} - N_{c_0}\right)\varphi + \left(\mathrm{I} + D'_{c_0} - D'_{c_1}\right)\psi. \end{aligned} \tag{4}$$

Throughout this article, we employ the Laplace Transform (LT)-based convolution quadrature (CQ)

method for time discretization, which we outline below using a frequency-domain (FD) operator theoretic approach. To this end, it is convenient to consider the following FD operator. For any known function $F : \mathbb{R}^d \to \mathbb{C}$ with support in $\overline{\Omega}$, and $z \in \mathbb{C}_+$, we define the solution operator $K(s)U$ as follows:

$$K(z)F = U, \quad \text{with} \left| \begin{array}{l} (z/c)^2 U(z) - \Delta u = F, \\ +\text{Radiation condition.} \end{array} \right. \tag{5}$$

The above solution operator $K(z)$ definition naturally extends to the case if the scalar z is replaced by a vector/matrix-valued function of z. In the latter case, the Helmholtz PDE needs to be solved for each z-dependent scalar component in the vector/matrix-valued counterpart. Such an extension is necessary for CQ methods based on A-stable Runge-Kutta (RK) ODE solvers.

For the special case of c as given in (1), the numerical counterpart of the LT-based FD operator $K(s)$ requires only the discretization of the LT counterparts of the BIOs mentioned above. In particular, we need to define the following FD BIOs using the fundamental solution $\widehat{G}(\kappa, z)$ of the Helmholtz equation, namely,

$$\widehat{G}(\kappa, \mathbf{z}) = \begin{cases} \dfrac{1}{4\pi\|\mathbf{z}\|} \exp(\mathrm{i}\kappa\|\mathbf{z}\|), & \text{in 3D}, \\ \dfrac{\mathrm{i}}{4} H_0^{(1)}(\kappa\|\mathbf{z}\|), & \text{in 2D}, \end{cases}$$

where $H_0^{(1)}(z)$) denotes the Hankel function of the first kind and zero order. Then, for $\mathbf{x} \in \partial\Omega$ we have

$$\mathcal{L}\left(S_k\right)\widehat{\varphi}(s,\mathbf{x}) = \int_{\partial\Omega} \widehat{G}\left(\frac{is}{k}, \mathbf{x}-\mathbf{y}\right)\widehat{\varphi}(\mathbf{y}) d\sigma(\mathbf{y}),$$

$$\mathcal{L}\left(D_k\right)\widehat{\psi}(s,\mathbf{x}) = \int_{\partial\Omega} \frac{\partial\widehat{G}}{\partial\boldsymbol{\nu}(\mathbf{y})}\left(\frac{is}{k}, \mathbf{x}-\mathbf{y}\right)\widehat{\psi}(\mathbf{y}) d\sigma(\mathbf{y}),$$

$$\mathcal{L}\left(D_k'\right)\widehat{\varphi}(s,\mathbf{x}) = \int_{\partial\Omega} \frac{\partial\widehat{G}}{\partial\boldsymbol{\nu}(\mathbf{x})}\left(\frac{is}{k}, \mathbf{x}-\mathbf{y}\right)\widehat{\varphi}(\mathbf{y}) d\sigma(\mathbf{y}),$$

$$\mathcal{L}\left(N_k\right)\widehat{\psi}(s,\mathbf{x})$$

$$= \int_{\partial\Omega} \frac{\partial^2\widehat{G}}{\partial\boldsymbol{\nu}(\mathbf{x})\partial\boldsymbol{\nu}(\mathbf{y})}\left(\frac{is}{k}, \mathbf{x}-\mathbf{y}\right)\widehat{\psi}(\mathbf{y}) d\sigma(\mathbf{y}).$$

The above hypersingular operator can be simplified using an integration by parts-type formula.

4. CONVOLUTION QUADRATURE METHOD

Denoting $\widehat{u}$ as the Laplace transform of u, we can express $u(t)$ using the Bromwich integral identity for the inverse Laplace transform:

$$\begin{aligned} u(t) &= \frac{1}{2\pi\mathrm{i}} \int_{\sigma+\mathrm{i}\mathbb{R}} \widehat{u}(t) e^{st}\, \mathrm{d}s \\ &= \frac{1}{2\pi\mathrm{i}} \int_{\sigma+\mathrm{i}\mathbb{R}} K(s) y(t;s)\, \mathrm{d}s, \qquad t \in [0,T], \end{aligned}$$

where K is the FD solution operator defined in (5), and $\sigma > 0$ is chosen appropriately. Here,

$$y(t;s) = \int_0^t f(\tau) e^{s(t-\tau)}\, \mathrm{d}\tau \tag{6}$$

solves the differential equation

$$x'(t) - sx(t) = f(t), \quad x(0) = 0, \quad t \in (0,T].$$

This approach forms the key idea behind the CQ method: it introduces an ODE solver to approximate $y(t;s)$ and reinterprets the Bromwich integral using complex integration techniques for analytic functions under suitable conditions. Hence, we have:

$$u(t) \approx \frac{1}{2\pi\mathrm{i}} \int_{\sigma+\mathrm{i}\mathbb{R}} e^{st} K\left(\frac{\widetilde{\delta}(e^{-\kappa s})}{\kappa}\right) F(s)\, \mathrm{d}s,$$

where $\widetilde{\delta}(\zeta)$ is the *so-called* approximate differentiation symbol of the ODE solver, and $\kappa > 0$ is the uniform time step. For example, in the simplest backward Euler ODE solver case, $\widetilde{\delta}(z) = 1 - z$, where z is a scalar. In the next section, for the case of RK ODE solver, we will precisely define a function $\widetilde{\delta}(\zeta)$ that we used in our implementation.

Expanding in a Taylor series for a suitable $0 < r < 1$:

$$K\left(\frac{\widetilde{\delta}(\zeta)}{\kappa}\right) = \sum_{j=0}^{\infty} w_j^{\kappa} \zeta^j,$$

where

$$w_j^{\kappa} = \frac{1}{2\pi\mathrm{i}} \int_{|\zeta|=r} \zeta^{-j-1} K\left(\frac{\widetilde{\delta}(\zeta)}{\kappa}\right) \mathrm{d}\zeta$$

we derive the representation:

$$\begin{aligned} u(n\kappa) &\approx \sum_{j=0}^{\infty} w_j^{\kappa} \int_{\sigma+i\mathbb{R}} e^{s(n\kappa-j)} F(s)\, \mathrm{d}s \\ &= \sum_{j=0}^{\infty} w_j^{\kappa} f((n-j)\kappa). \end{aligned}$$

Since $f(t) = 0$ for $t \leq 0$, the sum above is finite. If the weights w_j^κ are available or approximated, we observe that the method does not require the LT of f.

5. CQ-BEM AND CQ-FEM-BEM

5.1 RKCQ discretization in time

The applicability of the convolution quadrature (CQ) method, in conjunction with A-stable ODE solvers such as a special class of RK methods, hinges on the computation of the weights:

$$w_j^\kappa = \frac{1}{2\pi \mathrm{i}} \int_{|\zeta|=r} \zeta^{-j-1} K\left(\frac{\widetilde{\delta}(\zeta)}{\kappa}\right) \mathrm{d}\zeta \approx \frac{r^{-j}}{N+1} \sum_{\ell=0}^{N} e^{-\frac{2\pi j \mathrm{i}\ell}{N+1}} K(z_{\ell,n}^\kappa),$$

where we have used the rectangle rule to approximate the contour integral. This rule exhibits optimal convergence properties for such integrals. Here,

$$z_{\ell,N}^\kappa = \frac{1}{\kappa} \widetilde{\delta}\left(r e^{\frac{2\pi \mathrm{i}\ell}{N+1}}\right). \tag{7}$$

We note that N is chosen based on the final time T of the time-domain wave model, in combination with the uniform time-step parameter κ. More precisely, we have $T = (N+1)\kappa$.

Thus, we obtain the following continuous in space and discrete in time method:

$$u^{\kappa,N}(n\kappa) = \sum_{j=0}^{N} \frac{r^{j-n}}{N+1} \left[\sum_{\ell=0}^{N} e^{\frac{2\pi(n-j)\mathrm{i}\ell}{N+1}} K(z_{\ell,N}^\kappa) f(j\kappa)\right] = r^{-n} \sum_{\ell=0}^{N} e^{\frac{2\pi n \mathrm{i}\ell}{N+1}} K(z_{\ell,N}^\kappa) \left[\sum_{j=0}^{N} \frac{r^j}{N+1} e^{-\frac{2\pi j \mathrm{i}\ell}{N+1}} f(j\kappa)\right].$$

In this all-time-steps-at-once implementation of the CQ method, computing the solution at $N+1$ discrete times $\left(u^{\kappa,N}(n\kappa)\right)_{n=0}^{N}$ involves solving $N+1$ (vectorial) FD Helmholtz problems defined in (5), which facilitates natural parallelization. For the CQ-BEM case implementation, solving the FD problems corresponds to high-order discretizations of the associated BIOs defined in Section 3.

As previously mentioned, for time-discretization implementation, it is crucial to choose a precise formula to define the symbol $\widetilde{\delta}$ in (7) that corresponds to a numerical ODE solver capable of efficiently approximating the solution in (6). To this end, in this article, we choose an m-stage Radau II-A method, given by the Butcher tableau:

$$\begin{array}{c|c} \boldsymbol{c} & \boldsymbol{A} \\ \hline & \boldsymbol{b}^T, \end{array}$$

where $\boldsymbol{b}$ and $\boldsymbol{c}$ are $m \times 1$ column vectors, and $\boldsymbol{A}$ is an $m \times m$ matrix. Radau II-A methods are special cases of stiffly accurate A-stable and L-stable RK methods of order $2m-1$, with the constraint that the vector $\boldsymbol{c} = (c_l)_{1 \leq l \leq m}$ consists of the zeros (in ascending order) of the Radau polynomial. The entries of the matrix and vectors also satisfy two additional conditions, see for example [6, Section 3.1]. In this case, with $|\zeta| < 1$, we obtain

$$\widetilde{\delta}(\zeta) = \left(\boldsymbol{A} + \frac{\zeta}{1-\zeta} \mathbb{1} \boldsymbol{b}^T\right)^{-1}. \tag{8}$$

5.2 Spectral BEM and FEM-BEM discretization

First, we consider the piecewise-constant case in conjunction with the equivalent BIE system in (4). As described in [6], applying the RKCQ method to the time-domain BIE leads to a discrete system that possesses a lower triangular Toeplitz structure, which can be solved efficiently using a recursive scheme. Furthermore, the storage requirement can be reduced by leveraging the property that $\widetilde{\delta}(\zeta)$ is diagonalizable for almost every $|\zeta| < 1$.

For the spatial discretization of the Laplace transformed boundary integral operators, denoted as $\mathcal{L}(M)$ (with $M = S_k, D_k, D_k', N_k$), we utilize a spectrally accurate Kress-Nystrom method [10] specifically for the two-dimensional (2D) case. In this short article, we restrict our focus to the 2D scenario. (For the 3D case, we employ the spectrally accurate discretization approach presented in [11].)

For the general case involving heterogeneous media, we develop an overlapped time-domain CQ-FEM-BEM framework that facilitates the application of high-order FEM for bounded heterogeneous media and spectrally accurate BEM for unbounded free space. In the FD case, a similar FEM-BEM framework was developed and analyzed by the authors in [7, 8], introducing two artificial boundaries: one smooth boundary (suitable for spectral BEM) and another polygonal boundary (suitable for high-order FEM), as illustrated in Figure 2, which is exterior to an example bean-shaped domain Ω.

6. NUMERICAL EXPERIMENTS

In this section, we present numerical results to illustrate our CQ-BEM and CQ-FEM-BEM algorithms, which simulate time-domain wave propagation induced by a time-dependent incident wave given by

$$u^{\text{inc}}(t,\mathbf{x}) = \cos(\pi[t-\hat{\mathbf{d}}\cdot\mathbf{x}-2]^2) \times \exp\left(-\left[\frac{t-\hat{\mathbf{d}}\cdot\mathbf{x}-2}{0.4}\right]^2\right),$$

impinging upon the penetrable bean-shaped domain Ω from the incident direction $\hat{\mathbf{d}}$, where

$$\hat{\mathbf{d}} = \frac{\mathbf{d}}{\|\mathbf{d}\|}, \quad \text{with } \mathbf{d} = (1,-0.2).$$

We consider the time-domain model with $T = 8$. In the above example of the chosen incident wave, $u^{\text{inc}}(0,\cdot)$ does not strictly vanish in the bean-shaped domain $\overline{\Omega}$, as illustrated in Figure 2, and therefore does not exactly satisfy the conditions outlined in (2). However, since the values are are exponentially small in $\overline{\Omega}$, these can be treated as zero for computational purposes within this domain.

In addition to the domain Ω, Figure 2 illustrates our FEM-BEM framework: a coarse mesh for the rectangular region and a smooth simple curve Γ chosen to ensure that the unbounded region exterior to Γ represents a free-space with a constant speed of wave propagation ($c_0 = 1$). The rectangular region defined by $[-3,3]\times[-2,2]$ ensures that all heterogeneity is contained within the bounded region. The overlapped region, located between the blue curve Γ and the boundary of the rectangle (i.e., within the FEM domain but outside Γ), facilitates the coupling between the FEM solution in the interior and the BEM solution in the unbounded exterior. Such an overlapped coupling is crucial to efficiently solve first for unknowns on the two artificial boundaries, and then compute the CQ-FEM-BEM solution.

For comparison with the CQ-BEM approach, which ensures high-order accuracy, we consider the velocity field to be of the form given in (1) with $c_1 = 3.4$. Our CQ-BEM spectral algorithm does not require a mesh for the domain; instead, the spectral numerical solution is approximated using the Nyström quadrature rule [10, Eq. (3.94)] with $2n_{\text{per}}$ uniform knots on $\partial\Omega$. The refinement of the CQ-BEM time step κ necessitates boundary mesh refinement such that $(\kappa n_{\text{per}}) \approx 6$. However, our CQ-FEM-BEM framework does not impose such spatial and time discretization constraints. Let $n_{\text{CQ}} = N+1$, so that

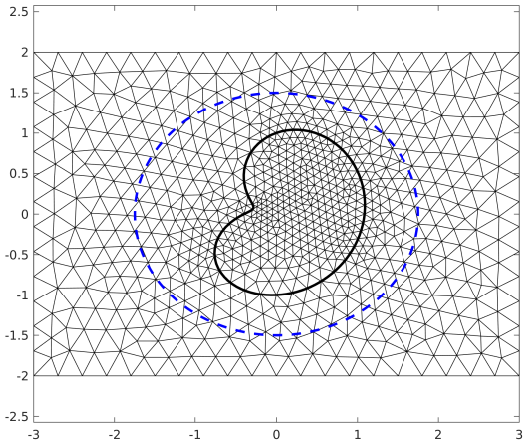

Figure 2. Bean-shaped penetrable domain Ω, with the overlapped region between $\partial\Omega$, an artificial smooth boundary Γ (in blue), and a coarse FEM method for the rectangular domain $[-3,3]\times[-2,2]$. The CQ-BEM approach formulates the integral equations on the true boundary $\partial\Omega$, while the CQ FEM-BEM method applies the FEM part of the algorithm on the rectangle and the BEM part on the (exterior of the) artificial boundary Γ, which are considerably simpler in nature.

$T = (n_{\text{CQ}})\times\kappa$. Therefore, in our numerical experiments, we set $\kappa = \frac{n_{\text{CQ}}}{8}$ for both the CQ-BEM and CQ-FEM-BEM algorithms, and we present our numerical results using the CQ parameter n_{CQ}. For our simulations, we employ the $m = 3$-stage RKCQ scheme for time discretization, with an expected order of convergence (EOC) of approximately 5.

For the CQ-BEM solution, once the BIE system in (4) is solved, we retrieve the total field solution to the wave equation in $\mathbb{R}^2\backslash\partial\Omega$ by again applying the accelerated RKCQ scheme to (3). The Frobenius-type norm errors $\mathbf{err}_{\text{Frob}}$ [6] between the CQ-BEM total field solution u^{κ}_{num} and a reference solution u^{*}_{num} are evaluated at $p = 100$ equi-spaced knots $(x_i)_{1\le i\le p}$ on two curves: one circle of radius 1.5 centered at the origin (located outside the domain Ω), and another circle of radius 0.5 centered at $(0.5,0)$ (located inside the domain Ω). The visual representation of these two circles (shown in dots) is provided in Figure 3. The reference solution u^{*}_{num} is computed with $N = 768$. In Table 1, we demonstrate the accuracy and the EOC of our CQ-BEM algorithm.

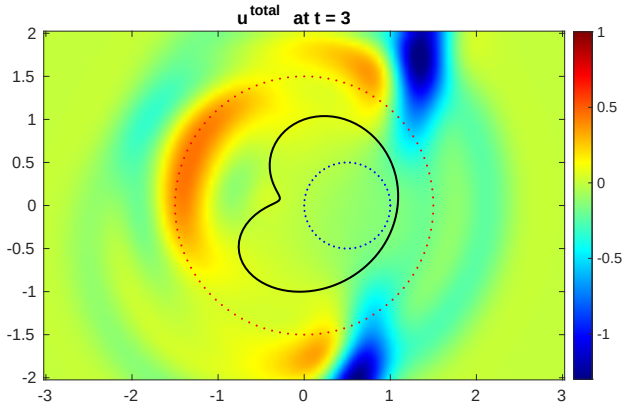

Figure 3. Numerical total field solution at $t = 3$ inside and exterior to the bean curve $\partial\Omega$. Interior and exterior numerical solution errors are evaluated at points, respectively, in the interior circle (in blue) inside Ω and the exterior circle (in red) exterior to Ω.

Table 1. Frobenius-type norm errors for the CQ-BEM total field solution u^{κ}_{num} w.r.t. to time step $\kappa = 8/N$ refinement on interval $[0, 8]$.

Exterior circle			Interior circle	
N	$\mathbf{err}_{\text{Frob}}$	EOC	$\mathbf{err}_{\text{Frob}}$	EOC
24	$7.21\text{E}-2$	–	$1.23\text{E}-1$	–
48	$5.43\text{E}-3$	3.73	$7.83\text{E}-3$	3.91
96	$2.06\text{E}-4$	4.71	$2.97\text{E}-4$	4.71
192	$7.49\text{E}-6$	4.78	$1.97\text{E}-5$	4.69

Having established the high-order accuracy of the CQ-BEM solution, we now demonstrate the high-order accuracy of the numerical solutions obtained using our new CQ-FEM-BEM framework, as illustrated in Figure 4.

In addition to the advantages presented by the CQ-FEM-BEM framework compared to the CQ-BEM approach (which is restricted to piecewise-constant velocity fields), our new framework facilitates the inclusion of a general heterogeneous medium Ω, with a complex structure. Furthermore, our CQ-FEM-BEM framework benefits from employing high-order BEM for unbounded regions with an exterior artificial smooth and simple boundary—such as the blue curve shown in Figure 2, instead of using BEM on the boundary of the penetrable object, which can be considerably complex in practice. Based on extensive experiments, it has been determined that

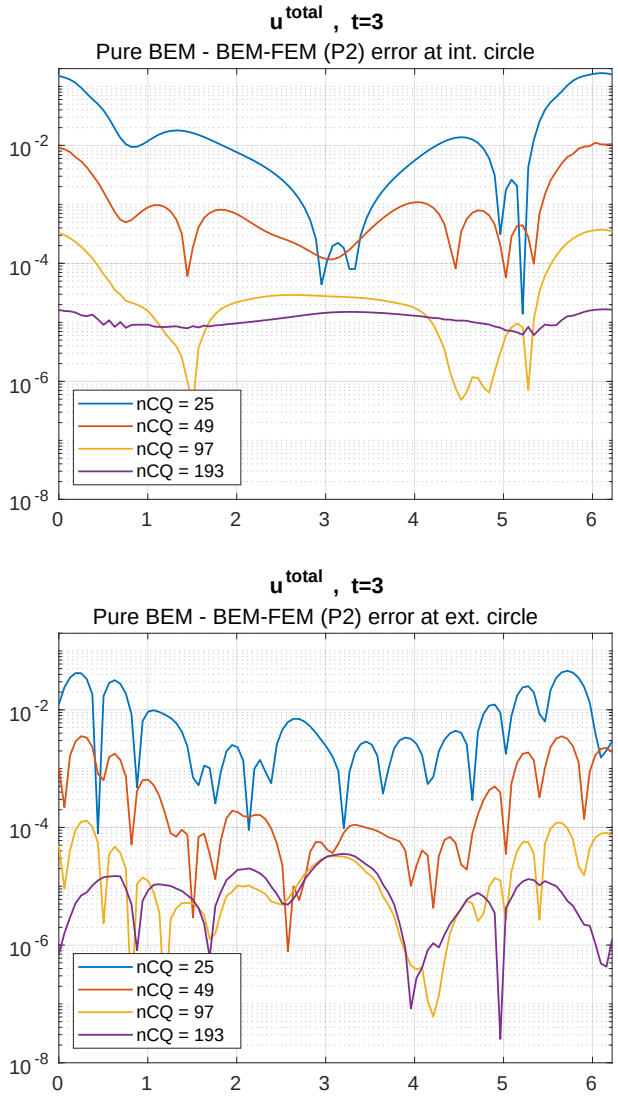

Figure 4. Error between the CQ-BEM (pure BEM) reference solution and CQ-FEM-BEM (FEM-BEM) solutions at $t = 3$ with varying CQ parameter $n_{\text{CQ}} = N + 1$ on the interior and exterior circles shown in Figure 3. The CQ-FEM-BEM solutions are computed on a fine FE mesh (the third refinement of the coarse mesh in Figure 2, comprising 58,348 elements) with quadratic ($\mathbb{P}_2$) splines.

our method does not require any spatial or temporal discretization constraints, unlike the CQ-BEM method. In future work, we will present our complete CQ-FEM-BEM

algorithm along with numerical analysis and comprehensive sets of experiments, which will include industry data-driven velocity field cases, such as the Marmousi velocity field.

7. REFERENCES

[1] M. Cheney and B. Borden, *Fundamentals of Radar Imaging*. SIAM, 2009.

[2] L. Banjai and F.-J. Sayas, *Integral Equation Methods for Evolutionary PDE: A Convolution Quadrature Approach*, vol. 59. Springer International Publishing, 2023.

[3] F. Ihlenburg, *Finite element analysis of acoustic scattering*, vol. 132 of *Applied Mathematical Sciences*. Springer-Verlag, New York, 1998.

[4] F.-J. Sayas, *Retarded potentials and time domain boundary integral equations: A roadmap*, vol. 50 of *Springer Series in Computational Mathematics*. Springer, [Cham], 2016.

[5] C. Lubich, "Convolution quadrature and discretized operational calculus. I," *Numer. Math.*, vol. 52, no. 2, pp. 129–145, 1988.

[6] M. Ganesh and F. Le Louër, "A high-order algorithm for time-domain scattering in three dimensions," *Adv. Comput. Math.*, vol. 49, no. 4, pp. Paper No. 46, 43, 2023.

[7] V. Domínguez, M. Ganesh, and F. J. Sayas, "An overlapping decomposition framework for wave propagation in heterogeneous and unbounded media: formulation, analysis, algorithm, and simulation," *J. Comput. Phys.*, vol. 403, pp. 109052, 20, 2020.

[8] V. Domínguez and M. Ganesh, "Analysis and application of an overlapped FEM-BEM for wave propagation in unbounded and heterogeneous media.," *Appl. Numer. Math.*, vol. 171, pp. 76–105, 2022.

[9] R. E. Kleinman and P. A. Martin, "On single integral equations for the transmission problem of acoustics," *SIAM J. Appl. Math.*, vol. 48, no. 2, pp. 307–325, 1988.

[10] D. Colton and R. Kress, *Inverse Acoustic and Electromagnetic Scattering Theory*. Springer, 4th ed., 2019.

[11] M. Ganesh and I. G. Graham, "A high-order algorithm for obstacle scattering in three dimensions," *J. Comput. Phys.*, vol. 198, no. 1, pp. 211–242, 2004.